ISSN (Online) 2394-2320

International Journal of Engineering Research in Computer Science and Engineering (IJERCSE)
Vol 4, Issue 12, December 2017

Advanced Control of DFIG for Wind Energy Conversion System Using Integrated Active Filter

[1] C.Mohan Krishna, [2] T.Manohar, [3] K Purushotham, [4] S.Imrankhan, [5] A.Venkata Prasad
[1] Assistant Professor, Anantha Lakshmi Institute of Technology and Sciences

Abstract - **Now a day's harmonics are serious problem in power systems. Due to non-linear loads being added to electrical systems harmonics are generated, which causes the system equipment damage. For improvement of power quality we are using DFIG with active filters. Doubly Fed Induction Generator for Wind Energy Conversion Systems deals with the operation of doubly fed induction generator (DFIG) with an integrated active filter capabilities using grid-side converter (GSC). The main contribution of this work lies in the control of GSC for supplying harmonics in addition to its slip power transfer. The rotor-side converter (RSC) is used for attaining maximum power extraction and to supply required reactive power to DFIG. Wind energy conversion system (WECS) works as a static compensator (STATCOM) for supplying harmonics even when the wind turbine is in shutdown condition. Control algorithms of both GSC and RSC are presented in detail. Implemented project DFIG-based WECS are simulated using MATLAB/Simulink.**

Keywords — Doubly fed induction generator (DFIG), Grid-side converter (GSC), Wind energy conversion system (WECS), Static compensator, rotor-side converter.

INTRODUCTION

With the increase in population and industrialization energy demand has increased significantly. Conventional energy sources such as coal, oil and gas are limited in nature. Renewable energy is energy generated from natural resources which are replenished such as wind, wave, solar, biomass and tidal power. Renewable energies are inexhaustible, clean and they can be used in a decentralized way (they can be used in the same place as they are produced). Also, they have the additional advantage of being complimentary, the integration between them being favourable. For example, solar photovoltaic energy supplies electricity on sunny days (in general with low wind) while on cold and windy days, which are frequently cloudy, the wind generators are in position to supply more electric energy.

In this paper, a new control algorithm for GSC (Grid Side Converter) is proposed for compensating harmonics produced by nonlinear loads using an indirect current control. RSC (Rotor side converter) is used for controlling the reactive power of DFIG. The other main advantage of proposed DFIG is that it works as an active filter even when the wind turbine is in shutdown condition. Therefore, it compensates load reactive power and harmonics at wind turbine stalling case. Both simulation and experimental performances of the proposed integrated active filter-based DFIG are presented in this work. The dynamic performance of the proposed DFIG is also demonstrated for varying wind speeds and changes in unbalanced nonlinear loads at point of common coupling (PCC). The system operation with improved power quality at point common coupling .However, the extensive use of power electronics based equipment and non-linear loads at point of common coupling generate harmonic currents, which may deteriorate the quality of power. Generally, current controlled voltage source inverters are used to interface the intermittent res in distributed system. Recently, a few control strategies for grid connected inverter incorporating power quality solution have been proposed. In an inverter operates as active inductor at a certain frequency to absorb the harmonic current. But the exact calculation of network inductance in real-time is difficult and may deteriorate the control performance. a similar approach in which a shunt active filter acts as active conductance to damp out the harmonic sin distribution network is proposed in [8]. In a control strategy for renewable interfacing inverter based on – theory is proposed. In this strategy both load and inverter current sensing is required to compensate the load current harmonics.

DFIG WIND BASED TURBINE:

Grid code requirements for the grid connection and operation of wind farms are discussed in [12]. Response of DFIG-based wind energy conversion system to grid disturbance is compared to the fixed speed WECS in [13]. As the wind penetration in the grid becomes significant, the use of variable speed WECS for supplementary jobs such as power smoothening and harmonic mitigation are compulsory in addition to its power generation. This power smoothening is achieved by including super magnetic energy storage systems as proposed in [14]. The other auxiliary services such as reactive power requirement and transient stability limit are achieved by including static compensator (STATCOM) in [15]. A distribution STATCOM (DSTATCOM) coupled with fly-wheel energy storage system is used at the wind farm for mitigating harmonics and frequency disturbances [16]. However, the authors have used two more extra converters for this purpose. A super capacitor energy storage system at the dc link of unified power quality conditioner (UPQC) is proposed in [17] for improving power quality and reliability. In all above methods [15]–[17], the authors have used separate converters for compensating the harmonics and also for controlling the reactive power. However, in later stages, some of the researchers have modified the control algorithms of already existed DFIG converters for mitigating the power quality problems and reactive power compensation [18]–[26]. The harmonics compensation and reactive power control are achieved with the help of existing RSC [18]–[23].Therefore, harmonics are injected from the RSC into the rotor windings. This creates losses and noise in the machine. These different harmonics in rotating part may also create mechanical unbalance. Moreover, both reactive power compensation and harmonic compensation are achieved in all these methods using RSC control. These methods increase the RSC rating. In [24] and [25], harmonic compensation and reactive power control are done using GSC. Therefore, the harmonics are not passing through machine windings in all these cases. Todeschiniand Emanuel [26] have compared three different control algorithms and finally concluded that combined modulation of both RSC and GSC are needed for compensating the harmonics and controlling the reactive power.

Block diagram for proposed system:

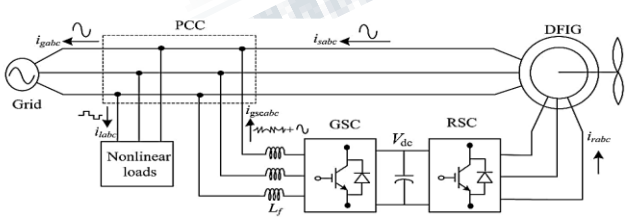

Proposed DFIG is that it works as an active filter even when the wind turbine is in shutdown condition. It compensates load reactive power and harmonics at wind turbine at stalling case. Total harmonics can be reduced. Reactive power can be compensated by local loads. Efficiency of the system is improved.

COMPARISON OF EXISTING AND PROPOSED SYSTEM:

Existing system	Proposed system
Direct current control technique	Indirect current control technique is used
THD is not less than 5%	THD can be effectively reduced below the 5%
It's not possible here	DFIG acts as an filter

DESIGN OF DFIG BASED WECS:

Selection of ratings of VSCs and dc-link voltage is very much important for the successful operation of WECS.

A. Selection of DC-Link Voltage:

Normally, the dc-link voltage of VSC must be greater than twice the peak of maximum phase voltage. The selection of dc-link voltage depends on both rotor voltage and PCC voltage. While considering from the rotor side, the rotor voltage is slip times the stator voltage. DFIG used in this prototype has stator to rotor turns ratio as 2:1. Normally, the DFIG operating slip is ±0.3. So, the rotor voltage is always less than the PCC voltage. So, the design criteria for the selection of dc-link voltage can be achieved by considering only PCC voltage. While considering from the GSC side, the PCC line voltage (vab) is 230 V, as the machine is connected in delta mode. The dc voltage link is estimated as

$$\mathbf{V_{dc}} \geq \frac{\mathbf{2\sqrt{2}}}{\mathbf{\sqrt{3} * m}} \mathbf{V_{ab}}$$

Where V_{ab} is the line voltage at the PCC. Maximum modulation index is selected as 1 for linear range. The value of dc-link voltage (V_{dc}) is estimated as 375 V.

B. Selection of VSC Rating:

The DFIG draws a lagging volt-ampere reactive (VAR) for its excitation to build the rated air gap voltage. It is calculated from the machine parameters that the

ISSN (Online) 2394-2320

International Journal of Engineering Research in Computer Science and Engineering (IJERCSE)

Vol 4, Issue 12, December 2017

lagging VAR of 2 KVAR is needed when it is running as a motor. In DFIG case, the operating speed range is 0.7 to 1.3 p.u. Therefore, the maximum slip (s_{max}) is 0.3. For making unity power factor at the stator side, reactive power of 600 VAR ($S_{max} * Q_s$= 0.3 ∗ 2 KVAR) is needed from the rotor side (Q_{rmax}). The maximum rotor active power is ($S_{max} * P$). The power rating of the DFIG is 5 kW. Therefore, the maximum rotor active power (P_{rmax}) is 1.5 kW (0.3 ∗ 5 kW = 1.5 kW). So, the rating of the VSC used as RSC S_{rated} is given as

$$\mathbf{S_{rated} = \sqrt{P_{rmax}^2 + Q_{rmax}^2}}$$

Thus, KVA rating of RSC Srated is calculated as 1.615 kVA

C. Design of Interfacing Inductor:

The design of interfacing inductors between GSC and PCC depends upon allowable GSC current limit (i_{gscpp}), dc-link voltage, and switching frequency of GSC. Maximum possible GSC line currents are used for the calculation. Maximum line current depends upon the maximum power and the line voltage at GSC. The maximum possible power in the GSC is the slip power. In this case, the slip power is 1.5 kW. Line voltage (V_L) at the GSC is 230 V (the machine is connected in delta mode). So, the line current is obtained as I_{gsc} = 1.5 kW/(√3 ∗ 230) = 3.765 A. Considering the peak ripple current as 25% of rated GSC current, the inductor value is calculated as below and Interfacing inductor between PCC and GSC is selected as 4 mH

$$\mathbf{L_i = \frac{\sqrt{3} m v_{dc}}{12 a f_m \Delta i_{gsc}}}$$

$$\mathbf{\frac{\sqrt{3}\times 1\times 375}{12\times 1.5\times 10000\times 0.25\times 3.76} = 3.8mH}$$

CONTROL STRATEGY:

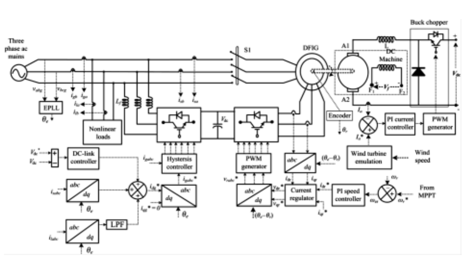

Fig.1. Control algorithm of the proposed WECS.

Control algorithms for both GSC and RSC are presented in this section. Complete control schematic is given in Fig. 3.1. The control algorithm for emulating wind turbine characteristics using dc machine and Type A chopper is also shown in above fig.

A. Control of RSC

The main purpose of RSC is to extract maximum power with independent control of active and reactive powers. Here, the RSC is controlled in voltage-oriented reference frame. Therefore, the active and reactive powers are controlled by controlling direct and quadrature axis rotor currents (idr and iqr), respectively. Direct axis reference rotor current is selected such that maximum power is extracted for a particular wind speed.

This can be achieved by running the DFIG at a rotor speed for a particular wind speed. Therefore, the outer loop is selected as a speed controller for achieving direct axis reference rotor (i_{dr}^*)

$$\boldsymbol{i_{dr}^*(k) = i_{dr}^*(k-1) + k_{pd}\{\omega_{er}(k) - \omega_{er}(k-1)\} + k_{id}\omega_{er}(k)}$$

Where the speed error (ωer) is obtained by subtracting sensed speed (ωr) from the reference speed (ω∗r). kpd and kid are the proportional and integral constants of the speed controller -ωer(k) and ωer(k − 1) are the speed errors at kth and (k−1)th instants. i_{dr}^*(k) and i_{dr}^*(k − 1) are the direct axis rotor reference current at kth and (k−1)th instants. Reference rotor speed (ω_r^*) is estimated by optimal tip speed ratio control for a particular wind speed.

The tuning of PI controllers used in both RSC and GSC are achieved using Ziegler Nichols method. Initially, kid value is set to zero and the value of kpd was increased until the response stars oscillating with a period of Ti Now, the value of kpd is taken as 0.45 kpd and kidis taken as 1.2 kpd/Ti.

Normally, the quadrature axis reference rotor current (i_{qr}^*) is selected such that the stator reactive power (Qs) is made zero. In this DFIG, quadrature axis reference rotor current (i_{qr}^*) is selected for injecting the required reactive power. Inner current control loops are taken for control of actual direct and quadrature axis rotor currents (idr and iqr) close to the direct and quadrature axis reference rotor currents (i_{dr}^* and i_{qr}^*). The rotor currents i_{dr} and iqr are calculated from the sensed rotor currents (ira, irb, and irc) as [32]

ISSN (Online) 2394-2320

International Journal of Engineering Research in Computer Science and Engineering (IJERCSE)
Vol 4, Issue 12, December 2017

$$i_{dr} = {}^{2}/_{3}\left[i_{ra}\sin\theta_{slip} + i_{rb}\sin(\theta_{slip} - {}^{2\pi}/_{3}) + i_{rc}\sin(\theta_{slip} + {}^{2\pi}/_{3})\right]$$

$$i_{qr} = {}^{2}/_{3}\left[i_{ra}\cos\theta_{slip} + i_{rb}\cos(\theta_{slip} - {}^{2\pi}/_{3}) + i_{rc}\cos(\theta_{slip} + {}^{2\pi}/_{3})\right]$$

Where slip angle is calculated as

$$\theta_{slip} = \theta_c - \theta_r$$

Where θ_e is calculated from PLL for aligning rotor currents into voltage axis. The rotor position (θ_r) is achieved with an encoder. Direct and quadrature axis rotor voltages ($v'_{dr}$and v'_{qr}) are obtained from direct and quadrature axis rotor current errors(i_{der} and i_{qer}) as

$$\mathbf{v'_{dr}(k) = v'_{dr}(k-1) + k_{pdv}\{i_{der}(k) - i_{der}(k-1)\} + k_{idv}i_{der}(k)}$$

$$\mathbf{v'_{qr}(k) = v'_{qr}(k-1) + k_{pqv}\{i_{qer}(k) - i_{qer}(k-1)\} + k_{iqv}i_{qer}(k)}$$

Where

$$\mathbf{i_{der} = i^*_{dr} - i_{dr} and i_{qer} = i^*_{qr} - i_{qr}}$$

Where k_{pdv} and k_{idv} are the proportional and integral gains of direct axis current controller, k_{pqv} and k_{iqv} are the proportional and integral gains of quadrature axis current controller Direct and quadrature components are decoupled by adding some compensating terms as[26]

$$v^*_{dr} = v'_{dr} + (\omega_e - \omega_r)\sigma L_r i_{qr}$$

$$v^*_{qr} = v'_{qr} - (\omega_e - \omega_r)(L_m i_{ms} + \sigma L_r i_{dr})$$

These reference direct and quadrature voltages ($\mathbf{v^*_{dr}, v^*_{qr}}$) are converted into three phase reference rotor voltages ($\mathbf{v_{ra}, v^*_{rb}, v^*_{rc}}$)as [32]

$$v^*_{ra} = v^*_{dr}\sin\theta_{slip} + v^*_{qr}\cos\theta_{slip}$$

$$v^*_{rb} = v^*_{dr}\sin(\theta_{slip} - {}^{2\pi}/_{3}) + v^*_{qr}\cos(\theta_{slip} - {}^{2\pi}/_{3})$$

$$v^*_{rc} = v^*_{dr}\sin(\theta_{slip} + {}^{2\pi}/_{3}) + v^*_{qr}\cos(\theta_{slip} + {}^{2\pi}/_{3})$$

These three phase rotor reference voltages (v^*_{ra}, v^*_{rb}, v^*_{rc}) are compared with triangular carrier wave of fixed switching frequency for generating pulse-width modulation (PWM) signals for the RSC.

B. Control of GSC

The novelty of this work lies in the control of this GSC for mitigating the harmonics produced by the nonlinear loads. The control block diagram of GSC is shown in Fig.3.1 Here; an indirect current control is applied on the grid currents for making them sinusoidal and balanced. Therefore, this GSC supplies the harmonics for making grid currents sinusoidal and balanced. These grid currents are calculated by subtracting the load currents from the summation of stator currents and GSC currents. Active power component of GSC current is obtained by processing the dc-link voltage error (v_{dc}) between reference and estimated dc link voltage (V^*_{dc} and V_{dc}) through PI controller as

$$\mathbf{i^*_{gsc}(k) = i^*_{gsc}(k-1) + k_{pdc}\{v_{dce}(k) - v_{dce}(k-1)\} + k_{idc}v_{dce}(k)}$$

Where k_{pdc} and k_{idc} are proportional and integral gains of the dc link. Vdce (k) and Vdc(k − 1) are dc link voltage errors at kth and (k−1)th instants. $i^*_{gsc}(k)$ and $i^*_{gsc}(k-1)$ are active power component of GSC current at kth and (k−1) th instants. Active power component of stator current (ids) is obtained from the sensed stator currents (i_{sa}, i_{sb}, and i_{sc}) using abcto dq transformation as [32]

$$i_{ds} = {}^{2}/_{3}\left[i_{sa}\sin\theta_e + i_{sb}\sin(\theta_e - {}^{2\pi}/_{3}) + i_{sc}\sin(\theta_e + 2\pi/3)\right]$$

Fundamental active load current ($\overline{i_{ld}}$) is obtained using SRF theory [33]. Instantaneous load currents (i_{labc}) and the value of phase angle from EPLL are used for converting the load currents in to synchronously rotating dq frame ($\widetilde{i_{ld}}$). In synchronously rotating frames, fundamental frequency currents are converted into dc quantities and all other harmonics are converted into non-dc quantities with a frequency shift of 50 Hz. DC values of load currents in synchronously rotating dq frame($\overline{i_{ld}}$) are extracted using low-pass filter (LPF). Direct axis component of reference grid current (i^*_{gd}) isobtained from the direct axis current

ISSN (Online) 2394-2320

International Journal of Engineering Research in Computer Science and Engineering (IJERCSE)
Vol 4, Issue 12, December 2017

of stator current (i_{ds}) and load current (i_{ld}) in synchronously rotating frame and the loss component of GSC current (i^*_{gsc}) as

$$\boldsymbol{i^*_{gd} = i^*_{gsc} + i_{ds} - \overline{i_{ld}}}$$

Quadrature axis component of reference grid current (i^*_{gq}) is selected as zero for not to draw any reactive power from grid. Reference grid currents (i^*_{ga}, i^*_{gb}, and i^*_{gc}) are calculated from the direct and quadrature axis grid currents (i∗gd, i∗gq) [32].

The hysteresis current controller is used to generate switching pulses for the GSC. The hysteresis controller is a feedback current control where sensed current tracks the reference current within a hysteresis band (i_{hb}) [34]. At every sampling instant, the actual current (i_{gabc}) is compared to the reference current (i^*_{gabc}) as

$$\Delta \boldsymbol{i_{gabc}} = \boldsymbol{i^*_{gabc}} - \boldsymbol{i_{gabc}}$$

When$\Delta \mathbf{i_{gabc}} > \mathbf{i_{hb}}$, lower switch is turned ON
When$\Delta \mathbf{i_{gabc}} < -\mathbf{i_{hb}}$, upper switch is turned ON.

Using these equations, gating pulses for three phases of GSC are generated in the same way.

SIMULATION and its RESULTS:
PROPOSED DFIG – BASED WECS AT FIXED WIND SPEED:

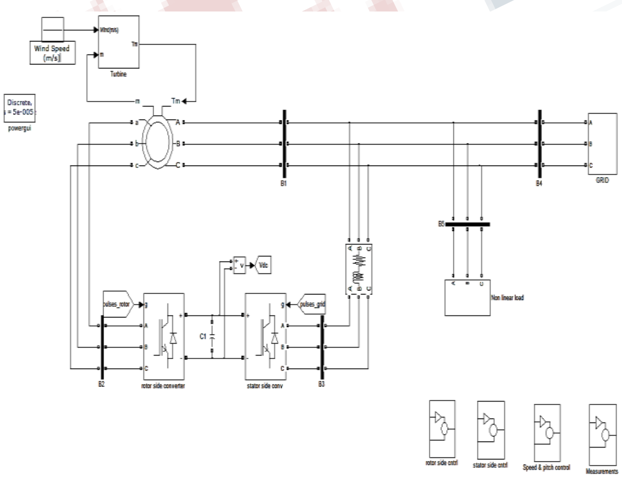

Fig 2: Block diagram of DFIG for WECS at fixed wind speed of 10.6 m/s

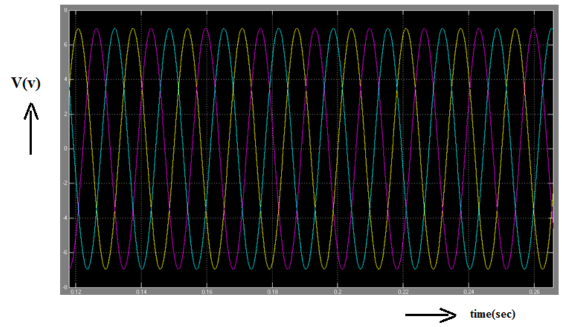

Fig(3) Vabc

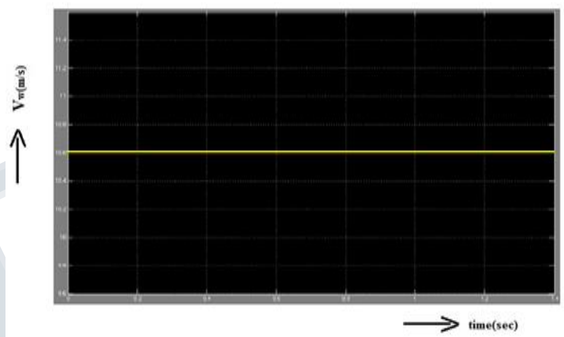

Fig(4) Fixed wind speed (10.6 m/s)

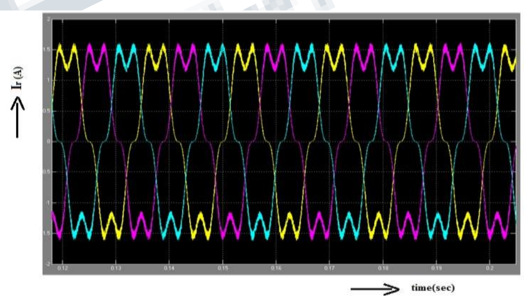

Fig(5)I_ abc_ rotor

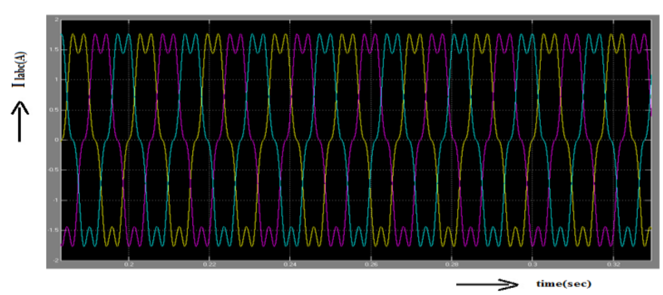

Fig(6) Currents at nonlinear loads

IFERP
connecting engineers... developing research
ISSN (Online) 2394-2320
International Journal of Engineering Research in Computer Science and Engineering (IJERCSE)
Vol 4, Issue 12, December 2017

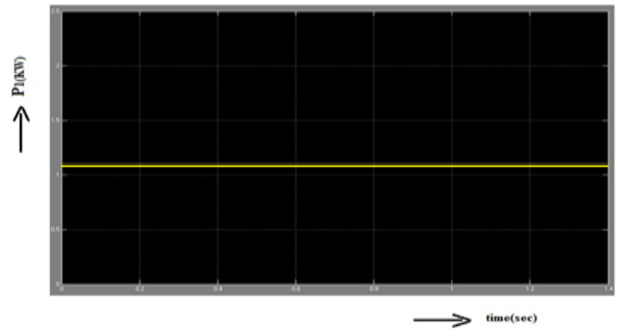

Fig(7) Power at nonlinear load

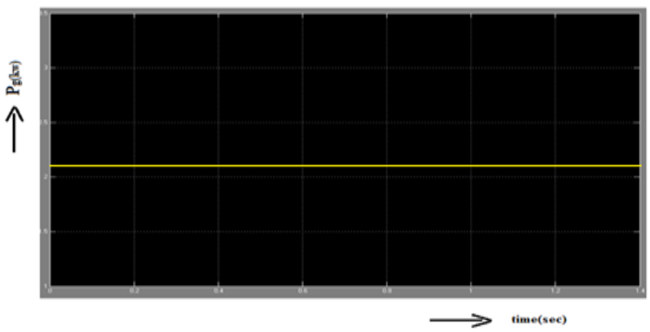

Fig(8) Power at grid

- Fig (3) the 3-Ø instantaneous load voltages at point of common of coupling. It is seen that the load end voltages are maintained constant and balanced irrespective of the non-linear loads. Time(s) is taken on x-axis and Vabc (v) is on y-axis.
- Fig (4) shows that the wind speed is fixed (10.6m/s) and it is constant at any time. The time(s) is taken on x-axis and wind speed (m/s) is on y-axis.
- Fig (5) represents the 3-Ø rotor currents ranging from 1.5 to -1.5A and its amplitude maintained constant throughout the time at the wind speed is constant. Time(s) is taken on x-axis and Ir(A) on y-axis.
- Fig (6) represents the 3-Ø sinusoidal current at non-linear load and it's ranging from 1.6 to -1.6A.The time is taken on x-axis and Ilabc on y-axis.
- Fig (7) shows the power at non-linear load (P1).The time(s) is taken on x-axis and P1 (kW) on y-axis. The power P1 (kw) is constant throughout the time. It's value is 1.1kw.
- Fig (8) shows the power at grid (Pg).It is also constant throughout the time, it's value is 2.1 kw.The Pg(kw) is taken on y-axis.

PROPOSED DFIG-BASED WECS WORKING AS STATCOM AT ZERO WIND SPEED:

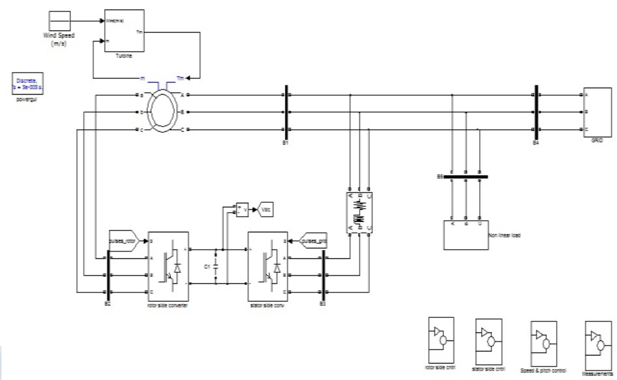

Fig 9: Block diagram of DFIG for WECS working as a STATCOM at zero wind speed

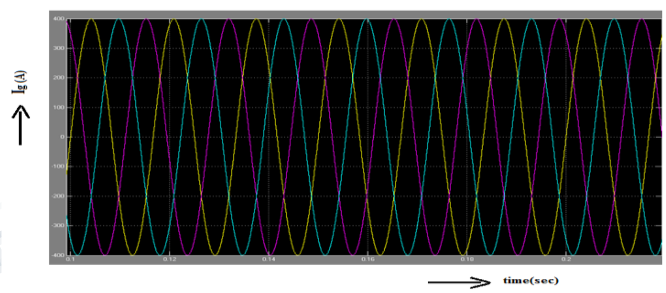

Fig (10) Grid current plot

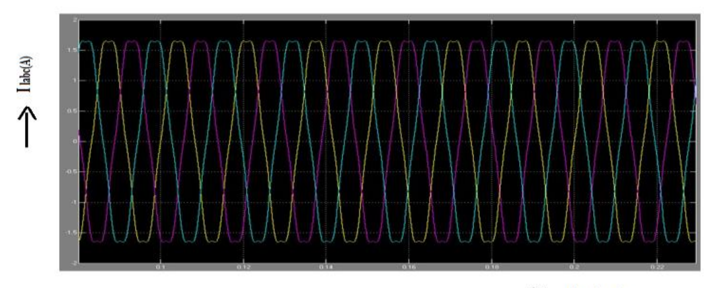

Fig (11) Rotor current

ISSN (Online) 2394-2320

International Journal of Engineering Research in Computer Science and Engineering (IJERCSE)
Vol 4, Issue 12, December 2017

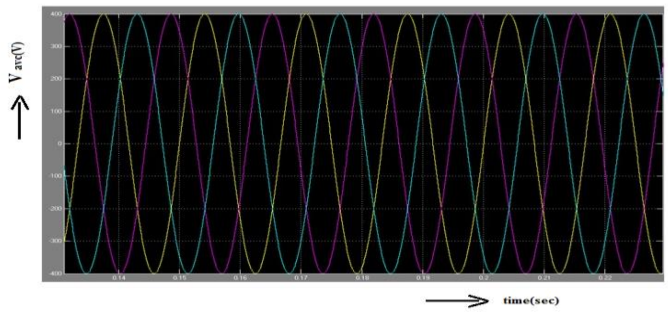

Fig (12) Voltage at nonlinear load

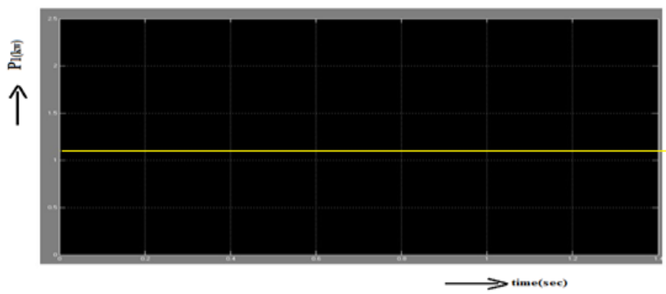

Fig (13) Power at nonlinear load

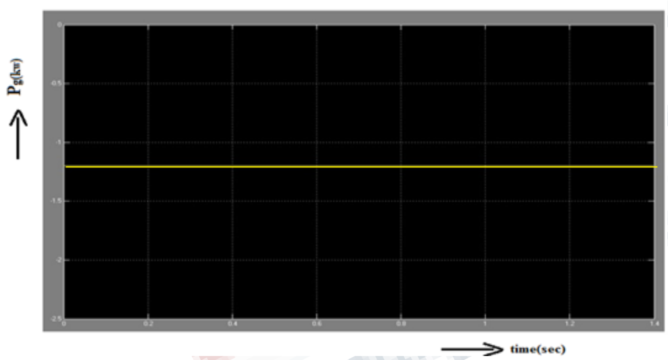

Fig (14) Reactive power at nonlinear load

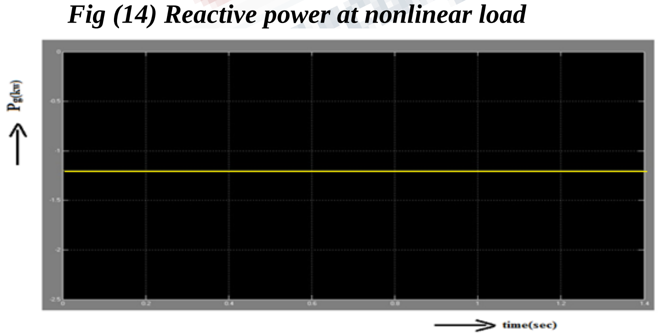

Fig (15) Active stator power grid

- Fig (10) shows the grid current ranging from 400 to -400 A. The grid current varies w.r.to time. It is seen like a pure sine wave. The time (sec) is taken on x-axis & Ig(A) on y-axis.
- Fig (11) shows the three phase rotor current ranging from 1.6 to -1.6A.The time(s) is taken on x-axis & Iabc on y-axis.
- Fig (12) represents the voltage at non-linear load ranging from 400 to -400V.The voltage is ranging w.r.to time. The Vabc is taken on y-axis.
- Fig (13) shows the power at non-linear load. It is constant at any time. When the wind speed is zero. The P1 (kw) is taken on y-axis. It's value is 1.1kw.
- Fig (14) shows the reactive power at non-linear load. The time(s) taken on x-axis and Q1 (kvar). It is constant throughout the time.
- Fig (15) represents active stator power grid. The time(s) taken on x-axis and Pg (kw) taken on y-axis.

PROPOSED DFIG FOR FALL IN WIND SPEED:

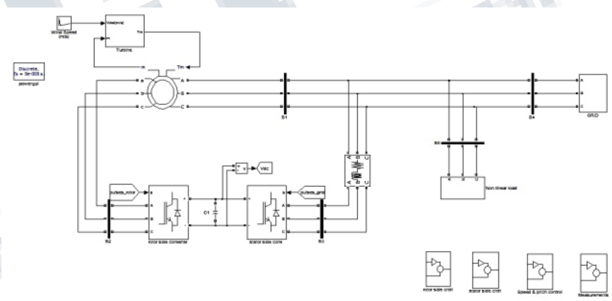

Fig16: Block diagram of DFIG for fall in wind speed

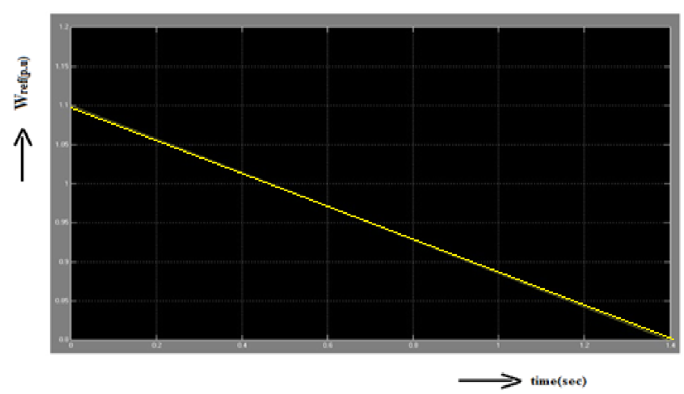

Fig (17) Fall in wind speed

ISSN (Online) 2394-2320

International Journal of Engineering Research in Computer Science and Engineering
(IJERCSE)
Vol 4, Issue 12, December 2017

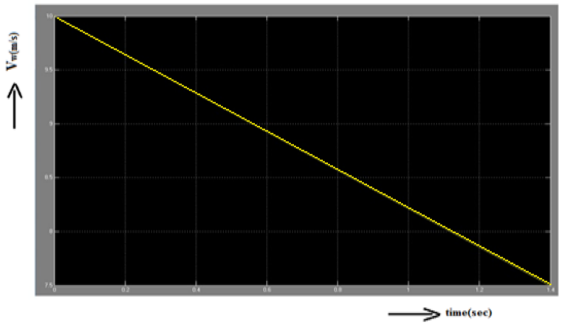

Fig (18) Wref

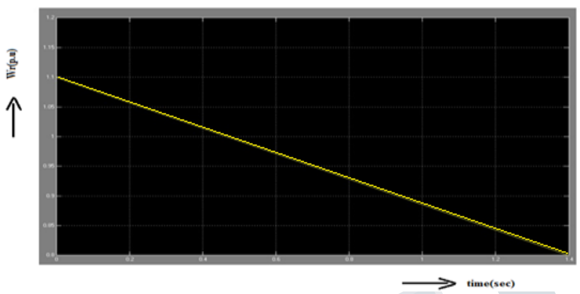

Fig (19) ω_r fall in rotor speed

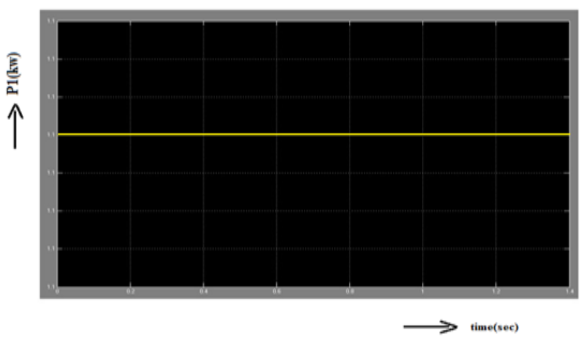

Fig (20)p_1 (Power at nonlinear load)

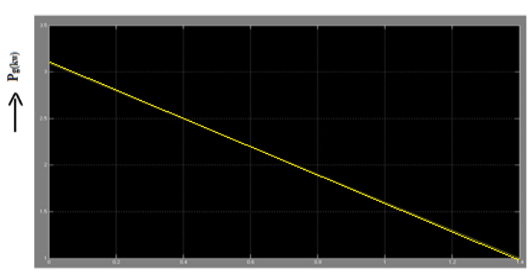

Fig (21)   (Power at stator grid)

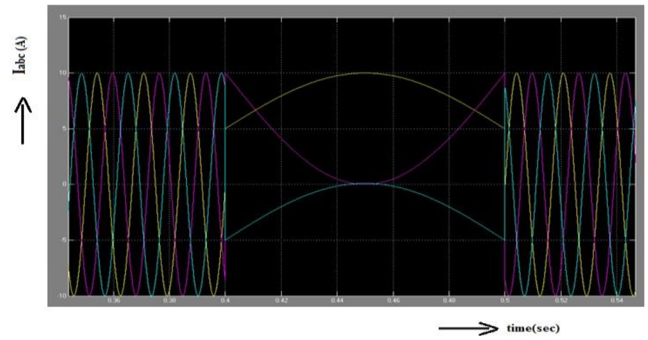

Fig (22) Iabc_stator

- Fig (17) represents the fall in wind speed. The wind is falling from10 (m/s) to 7.5 (m/s). The time (s) is taken on x-axis & Vw (m/s) is taken on y-axis.
- Fig (18) represents the Wref (p.u). its value is decreasing from 1.1 to 0.8 p.u
  The time(s) is taken on x-axis & Wref is taken on y-axis.
- Fig (19) shows that the fall in rotor speed. Rotor speed is falling from 1.1 to 0.8 p.u. The time(s) is taken on x-axis & Wr(p.u) is taken on y-axis.
- Fig (20) represents the power at non-linear load. It is constant through out the time. The time(s) is taken on x-axis & P1(kw) is on y-axis.
- Fig (21) represents the power at stator grid. Its value is falling from 3.1 (kw) to 1(kw). The time (sec) is taken on x-axis & Pg(kw) is on y-axis.
- Fig (22) shows that 3-Ø stator currents. Due to some disturbances the current wave form is distorted b/w the timings from 0.4(s) to 0.5(s). The time(s) is taken on x-axis & Irabc (A) is on y-axis.

CONCLUSION:

The GSC control algorithm of the proposed DFIG has been modified for supplying the harmonics and reactive power of the local loads. In this proposed DFIG, the reactive power for the induction machine has been supplied from the RSC and the load reactive power has been supplied from the GSC. The decoupled control of both active and reactive powers has been achieved by RSC control. The proposed DFIG has also been verified at wind turbine stalling condition for compensating harmonics and reactive power of local loads.

This proposed DFIG-based WECS with an integrated active filter has been simulated using MATLAB/Simulink environment, and the simulated results are presented. Dynamic performance of this proposed GSC control algorithm has also been verified for the variation in the wind speeds and for local nonlinear load.

FUTURE SCOPE:

The controller can be modified and implemented in fuzzy logic controller. The simulation result of FLC can be most steady state and fast response.

REFERENCES:

[1] D. M. Tagare, Electric Power Generation the Changing Dimensions. Piscataway, NJ, USA: IEEE Press, 2011.

[2] G. M. Joselin Herbert, S. Iniyan, and D.Amutha, “A review of technical issues on the development of wind farms,” Renew. Sustain. Energy Rev.,vol. 32, pp. 619–641, 2014.

[3] I.Munteanu, A. I. Bratcu, N.-A. Cutululis, and E. Ceang, Optimal Control of Wind Energy Systems Towards a Global Approach. Berlin, Germany: Springer-Verlag, 2008.

[4] A. A. B. MohdZin, H. A. Mahmoud Pesaran, A. B. Khairuddin, L. Jahanshaloo, and O. Shariati, “An overview on doubly fed induction generators controls and contributions to wind based electricity generation,” Renew. Sustain. Energy Rev., vol. 27, pp. 692–708, Nov. 2013.

[5] S. S. Murthy, B. Singh, P. K. Goel, and S. K. Tiwari, “A comparative study of fixed speed and variable speed wind energy conversion systems feeding the grid,” in Proc. IEEE Conf. Power Electron. Drive Syst. (PEDS’07), Nov. 27–30, 2007, pp. 736–743.

[6] D. S. Zinger and E. Muljadi, “Annualized wind energy improvement using variable speeds,” IEEE Trans. Ind. Appl., vol. 33, no. 6, pp. 1444– 1447, Nov./Dec. 1997.

[7] H. Polinder, F. F. A. van der Pijl, G. J. de Vilder, and P. J. Tavner, “Comparison of direct-drive and geared generator concepts for wind turbines,” IEEE Trans. Energy Convers., vol. 21, no. 3, pp. 725–733,Sep. 2006.

[8] R. Datta and V. T. Ranganathan, “Variable-speed wind power generation using doubly fed wound rotor induction machine—A comparison with alternative schemes,” IEEE Trans. Energy Convers., vol. 17, no. 3, pp. 414–421, Sep. 2002.

[9] E. Muljadi, C. P. Butterfield, B. Parsons, and A Ellis, “Effect of variable speed wind turbine generator on stability of a weak grid,” IEEE Trans. Energy Convers., vol. 22, no. 1, pp. 29–36, Mar. 2007.

[10] R. Pena, J. C. Clare, and G. M. Asher, “Doubly fed induction generator using back-to-back PWM converters and its application to variable-speed wind-energy generation,” IEE Proc. Elect. Power Appl., vol. 143, no. 3,pp. 231–241, May 1996.

[11] S. Muller, M. Deicke, and R. W. DeDoncker, “Doubly fed induction generator systems for wind turbines,” IEEE Ind. Appl. Mag., vol. 8, no. 3, pp. 26–33, May/Jun. 2002.

[12] W. Qiao and R. G. Harley, “Grid connection requirements and solutions for DFIG wind turbines,” in Proc. IEEE Energy 2030 Conf.(ENERGY’08), Nov. 17–18, 2008, pp. 1–8.

[13] A. Petersson, T. Thiringer, L. Harnefors, and T. Petru, “Modeling and experimental verification of grid interaction of a DFIG wind turbine,” IEEE Trans. Energy Convers., vol. 20, no. 4, pp. 878–886, Dec. 2005.

[14] H. M. Hasanien, “A set-membership affine projection algorithm-based adaptive-controlled SMES units for wind farms output power smoothing,”IEEE Trans. Sustain. Energy, vol. 5, no. 4, pp. 1226–1233, Oct. 2014.

[15] Z. Saad-Saoud, M. L. Lisboa, J. B. Ekanayake, N. Jenkins, and G. Strbac,“Application of STATCOMs to wind farms,” IEE Proc. Gener. Transmiss.Distrib., vol. 145, no. 5, pp. 511–516, Sep. 1998.

[16] G. O. Suvire and P. E. Mercado, “Combined control of a distribution static synchronous compensator/flywheel energy storage system for wind energy applications,” IET Gener. Transmiss.Distrib., vol. 6, no. 6, pp. 483–492, Jun. 2012.

[17] D. Somayajula and M. L. Crow, “An ultra capacitor integrated power conditioner for intermittency smoothing

and improving power quality of distribution grid," IEEE Trans. Sustain. Energy, vol. 5, no. 4, pp. 1145–1155, Oct. 2014.

[18] M. T. Abolhassani, P. Enjeti, and H. Toliyat, "Integrated doubly fed electric alternator/active filter (IDEA), a viable power quality solution, for wind energy conversion systems," IEEE Trans. Energy Convers., vol. 23, no. 2, pp. 642–650, Jun. 2008.

[19] A. Gaillard, P. Poure, and S. Saadate, "Active filtering capability of WECS with DFIG for grid power quality improvement," in Proc. IEEE Int. Symp. Ind. Electron., Jun. 30, 2008, pp. 2365–2370.

[20] A. Gaillard, P. Poure, and S. Saadate, "Reactive power compensation andactive filtering capability of WECS with DFIG without any overrating,"Wind Energy, vol. 13, pp. 603–614, 2009.

[21] M. Boutoubat, L. Mokrani, and M. Machmoum, "Control of a wind energy conversion system equipped by a DFIG for active power generation and power quality improvement," Renew. Energy, vol. 50, pp. 378–386, Feb. 2013.

[22] A. Ejlali and D. Arab Khaburi, "Power quality improvement using nonlinear-load compensation capability of variable speed DFIG based on DPC-SVM method," in Proc. 5th Power Electron. Drive Syst. Technol. Conf. (PEDSTC), Feb. 5–6, 2014, pp. 280–284.

[23] B. Mohamed, L. Mokrani, and M. Machmoum, "Full capability of harmonic current mitigation for a wind energy system," Elect. Power Comp. Syst., vol. 42, no. 15, pp. 1743–1753, 2009.

[24] E. Tremblay, A. Chandra, and P. J. Lagace, "Grid-side converter control of DFIG wind turbines to enhance power quality of distribution network," in Proc. IEEE PES Gen. Meeting, 2006, p. 6.

[25] E. Tremblay, S. Atayde, and A Chandra, "Direct power control of a DFIG-based WECS with active filter capabilities," in Proc. IEEE Elect. Power Energy Conf. (EPEC), Oct. 22–23, 2009, pp. 1–6.

[26] G. Todeschini and A. E. Emanuel, "Wind energy conversion system as an active filter: Design and comparison of three control systems," IET Renew. Power Gener., vol. 4, no. 4, pp. 341–353, Jul. 2010.

[27] B. N. Singh, A. Chandra, and K. Al-Haddad, "Performance comparison of two current control techniques applied to an active filter," in Proc. 8th Int. Conf. Harmonics Qual. Power Proc., Oct. 14–18, 1998, vol. 1, pp. 133–138.

[28] B. N. Singh, A. Chandra, and K. Al-Haddad, "DSP-basedindirectcurrent- controlled STATCOM. I. Evaluation of current control techniques," IEE Proc. Elect. Power Appl., vol. 147, no. 2, pp. 107–112,Mar. 2000.

[29] B. N. Singh, A. Chandra, and K. Al-Haddad, "DSP-based indirectcurrent-controlled STATCOM. II. Multifunctional capabilities," IEE Proc. Elect.Power Appl., vol. 147, no. 2, pp. 113–118, Mar.2000.

[30] B. N. Singh, B. Singh, A. Chandra, P.Rastgoufard, and K. Al-Haddad, "An improved control algorithm for active filters," IEEE Trans. Power Del., vol. 22, no. 2, pp. 1009–1020, Apr. 2007.

[31] S. Sharma and B. Singh, "Voltage and frequency control of asynchronous generator for stand-alone wind power generation," IET Power Electron.,vol. 4, no. 7, pp. 816–826, Aug. 2011.

[32] G. Abad, J. López, M. Rodríguez, L. Marroyo, and G. Iwanski, Doubly Fed Induction Machine: Modeling and Control for Wind Energy Generation Applications. Hoboken, NJ, USA: Wiley\IEEE Press,2011.

[33] B. Singh and J. Solanki, "A comparison of control algorithms for DSTATCOM," IEEE Trans. Ind. Elect., vol. 56, no. 7, pp. 2738–2745, Jul. 2009.

[34] B. K. Bose, Modern Power Electronics and AC Drives, 4th ed. Englewood Cliffs, NJ, USA: Prentice-Hall, 2007, ch. 5.

[35] IEEE Recommended Practices and Requirements for Harmonic Control in Electrical Power Systems, IEEE Standard 519, 1992.